

First Results of Searches for New Physics at $\sqrt{s}=7$ TeV with the CMS detector

Paolo Azzurri

Scuola Normale Superiore, Piazza dei Cavalieri 7, 56126 Pisa, Italy

E-mail: paolo.azzurri@cern.ch

Abstract. First searches for new physics phenomena using the LHC 7 TeV proton-proton collision data collected by the CMS detector in 2010 are reviewed. Results are presented of searches for new physics in events with hadronic jet pairs, and for heavy stable charged particles, including a dedicated search for long-lived particles that stop in the detector and decay in periods between beam crossings.

1. Introduction

During the 2010 LHC running, the CMS experiment [1] recorded over 40 pb^{-1} of pp collisions at 7 TeV center-of-mass energy. The large momentum transfers accessible at these collision energies allow to test for new short range physics scenarios beyond the predictions of Quantum Chromodynamics (QCD) in dijet events, and to search for the production of new heavy quasi-stable particles [2].

In the following, results for the search of new physics in dijet events are presented for resonances in the dijet mass spectrum in Section 2, and for new interactions affecting dijet angular distributions in Sections 3 and 4. The outcome of searches for generic heavy stable charged particles are given in Section 5, while the pursuit of long-lived gluinos that stop and decay in the CMS detector is detailed in Section 6.

2. Narrow dijet resonances

In proton-proton collisions QCD predicts that the invariant mass spectrum of the two jets with largest p_T falls steeply and smoothly, while new massive objects that couple to quarks (q) and gluons (g) would show up as resonant structures in the dijet mass. A data sample of $2.9 \pm 0.3 \text{ pb}^{-1}$ is employed for this analysis [3], using a single-jet trigger with a transverse energy threshold of 50 GeV, that is measured to be over 99.5% efficient for dijet masses above 220 GeV.

Jets are reconstructed with the anti- k_T algorithm [4] and $R = 0.7$. The reconstructed jet energy E is corrected as a function of p_T and η for the non-linearity and inhomogeneity of the calorimeter response [5]. The two jets with the leading p_T define the dijet system. The inclusive dijet mass is shown in Figure 1, where the data points are compared with a prediction from PYTHIA [6], that is in agreement within the 10% jet energy scale uncertainty. The data is also compared with a smooth fit to a functional form with four free parameters, and there is no indication of narrow resonances.

The dijet mass data points, the fitted background parameterization, and the expected dijet resonance shapes are used to set specific Bayesian limits on new particles decaying to parton

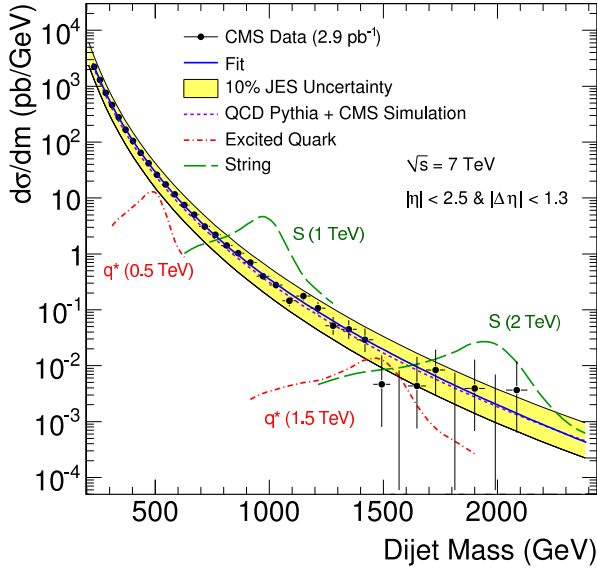


Figure 1. Dijet mass spectrum. The data points are superimposed with a smooth fit (solid line) and to QCD predictions [6] (short-dashed line). The shaded band shows the jet energy scale uncertainty. Possible excited quark signals and string resonance signals are also shown.

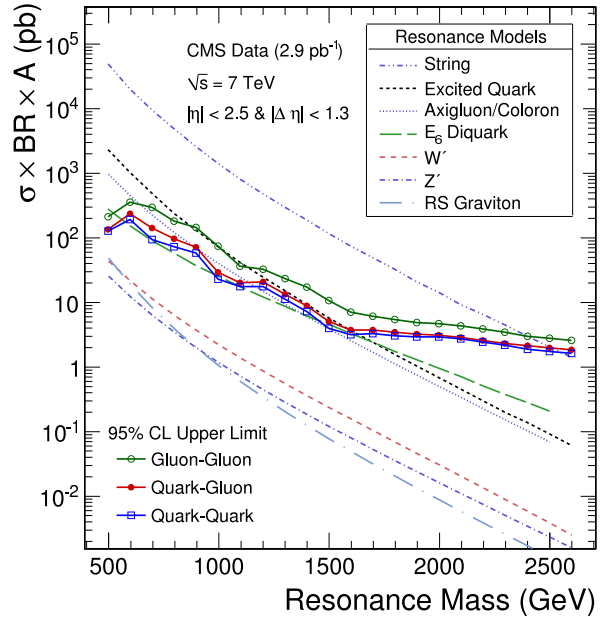


Figure 2. Production upper limits for resonances decaying to gluon-gluon, quark-gluon, and quark-quark dijets, compared to theoretical predictions from different models.

pairs. The obtained 95% confidence level (CL) upper limits on the resonances production are shown in Figure 2 and compared to the expected productions in different models. The resulting excluded mass ranges for string resonances [7], excited quarks [8], axigluons [9], colorons [10] and E_6 diquarks [11] all extend previous exclusions [3], while for new gauge bosons W' and Z' [12], and Randall-Sundrum gravitons [13] no mass interval is excluded with the present data.

3. Dijet centrality ratio

In proton-proton collisions the QCD dijet production is dominated by t-channel processes and peaks in the forward direction (along the beam axis) while new physics scenarios, including models of quark compositeness, predict more isotropic angular distribution, leading to enhanced jet production at smaller pseudorapidity values.

The dijet centrality ratio R_η between the number of events with the two leading jets in the region $|\eta| < 0.7$ and the number of events with the two jets in the region $0.7 < |\eta| < 1.3$, is defined to use less angular information than a full dijet angular distribution analysis, but allows for fine binning in the dijet mass and cancels many sources of systematic uncertainty, providing an accurate test of QCD and probe to new physics. The analysis [14] is based on the same data sample, events selection and jet reconstruction used for the previously described dijet resonances search [3]. Figure 3 shows the predicted and observed values of R_η as a function of the dijet mass m_{jj} . The measured R_η is nearly flat with a value of about 0.5, as predicted by QCD, while the presence of quark contact interactions would lead to an increase of R_η above a value of m_{jj} that depends on the compositeness energy scale Λ .

A log-likelihood-ratio \mathcal{R}_{LL} is used to test for the presence of quark compositeness, and, given the consistency of the data with the QCD hypothesis, a modified frequentist method with the

CL_s approach [15], is employed to derive the 95% CL limit $\Lambda > 4.0$ TeV , as displayed in Figure 4

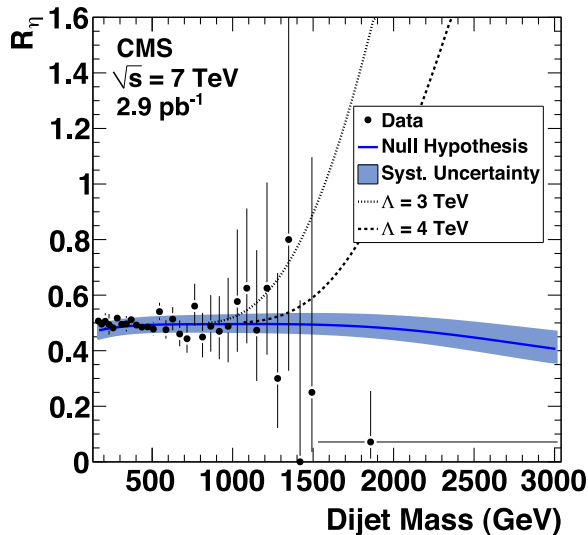


Figure 3. The observed dijet centrality ratio as a function of m_{jj} compared with QCD predictions (solid line), with the systematic uncertainty band, and to two hypotheses of quark contact interactions with $\Lambda = 3, 4$ TeV.

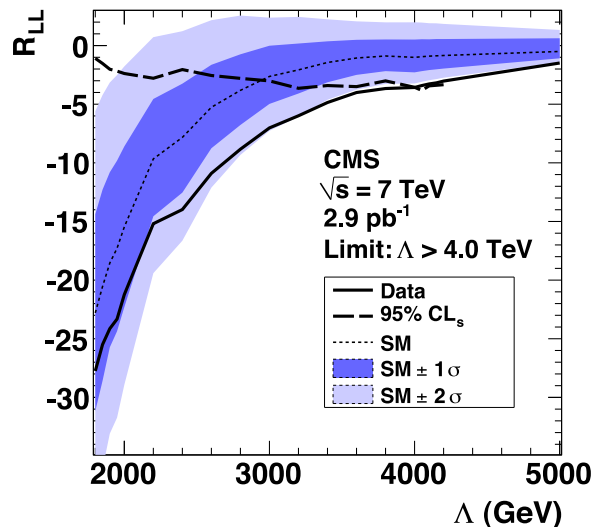


Figure 4. Exclusions for the contact interaction scale Λ . We show \mathcal{R}_{LL} versus Λ for the data (solid line), the 95% CL_s (dashed line), and the SM expectation (dotted line) with 1σ (dark) and 2σ (light) bands.

4. Dijet angular distributions

The complete dijet angular distribution is measured through the differential cross section $(1/\sigma_{\text{dijet}})(d\sigma_{\text{dijet}}/d\chi_{\text{dijet}})$ where $\chi_{\text{dijet}} = (1 + |\cos \theta^*|)/(1 - |\cos \theta^*|)$, and θ^* is the polar scattering angle in the dijet center-of-mass (CM) frame [16]. This choice is motivated by the fact that $d\sigma_{\text{dijet}}/d\chi_{\text{dijet}}$ is rather flat for QCD (Rutherford) parton scattering.

A data sample of up $36 \pm 4 \text{ pb}^{-1}$ is employed for this analysis, and events are selected with five inclusive single-jet triggers, with different jet transverse momentum p_T thresholds. Offline jets are reconstructed with the anti- k_T algorithm [4] with $R = 0.5$, and the reconstructed jet energy is corrected [5]. The differential dijet angular distributions for different m_{jj} ranges, normalized to their respective integrals, are shown in Fig. 5. The data are compared with perturbative QCD (pQCD) predictions at next-to-leading order (NLO), for all m_{jj} ranges.

Given the good agreement with pQCD, the data are used to set limits on quark compositeness represented by a four-fermion contact interaction term in addition to the QCD Lagrangian. As in the previous section, a statistical test based on the log-likelihood-ratio \mathcal{R}_{LL} is used to derive limits on Λ , using the modified frequentist CL_s approach [15]. The results are shown in Figure 6, and a 95% confidence level bound $\Lambda > 5.6$ TeV is observed, the currently most stringent limit on the contact interaction scale of left-handed quarks.

5. Heavy Stable Charged Particles

Many extensions of the standard model predict the existence of heavy (quasi-)stable charged particles (HSCPs), that would travel across the size of typical particle detector [2], and could be observable as high momentum (p) particles with exceptional ionization energy loss (dE/dx).

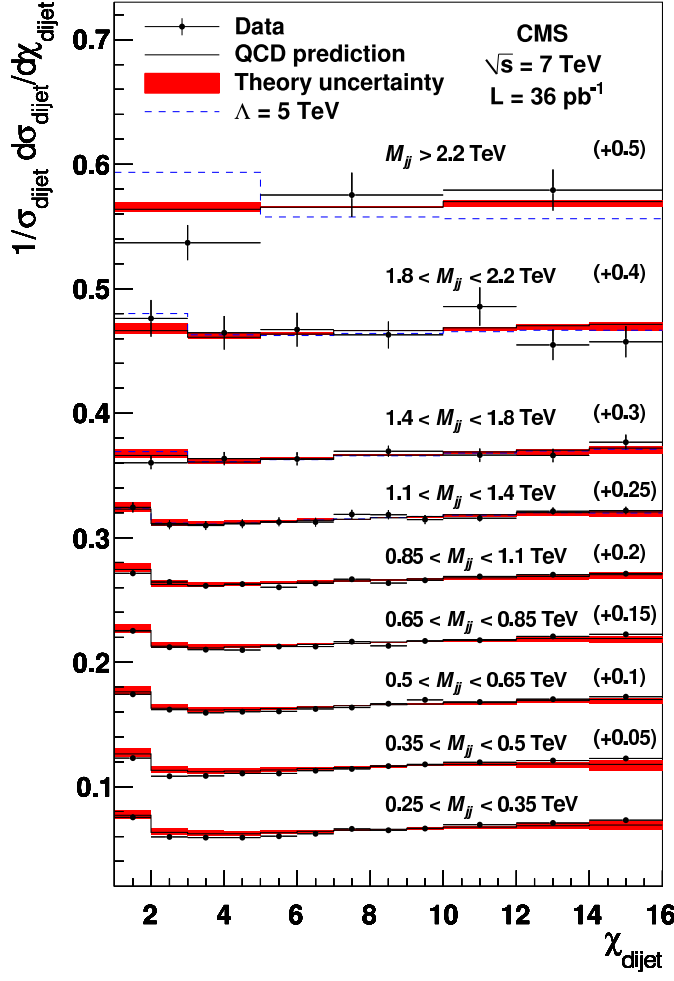


Figure 5. Normalized dijet angular distributions in m_{jj} ranges, shifted vertically (as given in parentheses) for clarity. The data points include full uncertainty bars and are compared with the predictions of pQCD at NLO (solid histogram) and with the predictions including a contact interaction term of compositeness scale $\Lambda = 5$ TeV (dashed histogram). The shaded band shows the effect on the NLO pQCD predictions due to factorization and renormalization scale variations and parton distribution functions uncertainties, as well as the uncertainties from the non-perturbative corrections added in quadrature.

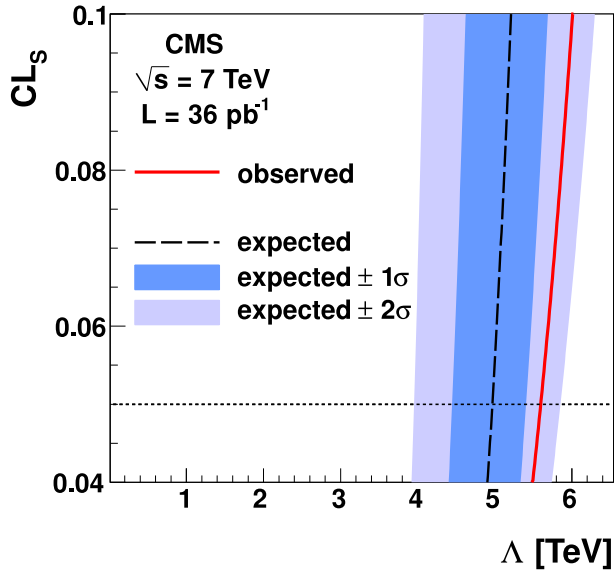


Figure 6. The observed CL_s (solid) and expected CL_s (dashed) with one (two) standard deviation indicated by the dark (light) band as a function of the contact interaction scale Λ , from the dijet angular distributions. The 95% confidence level limits on Λ are extracted from the intersections of the CL_s lines with the horizontal line at $CL_s = 0.05$.

The CMS search [17] is based on an integrated luminosity of 3.1 pb^{-1} , and has two approaches. A “tracker-only” selection looks for charged particles in the inner tracker with large dE/dx and

p_T . A “*tracker-plus-muon*” selection additionally requires associated hits in the outer muon detectors. For both selections, the mass of the candidate is estimated from the measured p and dE/dx . For candidate tracks with $|\eta| < 2.5$ and $p_T > 15$ GeV/ c , an estimator I_{as} of the degree of compatibility of the observed charge measurements in the silicon detector with the minimum-ionizing particle (MIP) hypothesis is used to point out non-relativistic HSCP candidates. The data and Monte Carlo (MC) normalized distributions of p_T and I_{as} for pre-selected tracker-only candidates are shown in Figure 7. One MC sample contains events from standard QCD processes, while the second MC sample contains signal events from pair-production of stable \tilde{g} with a mass of 200 GeV/ c^2 . Both samples are generated with PYTHIA [6].

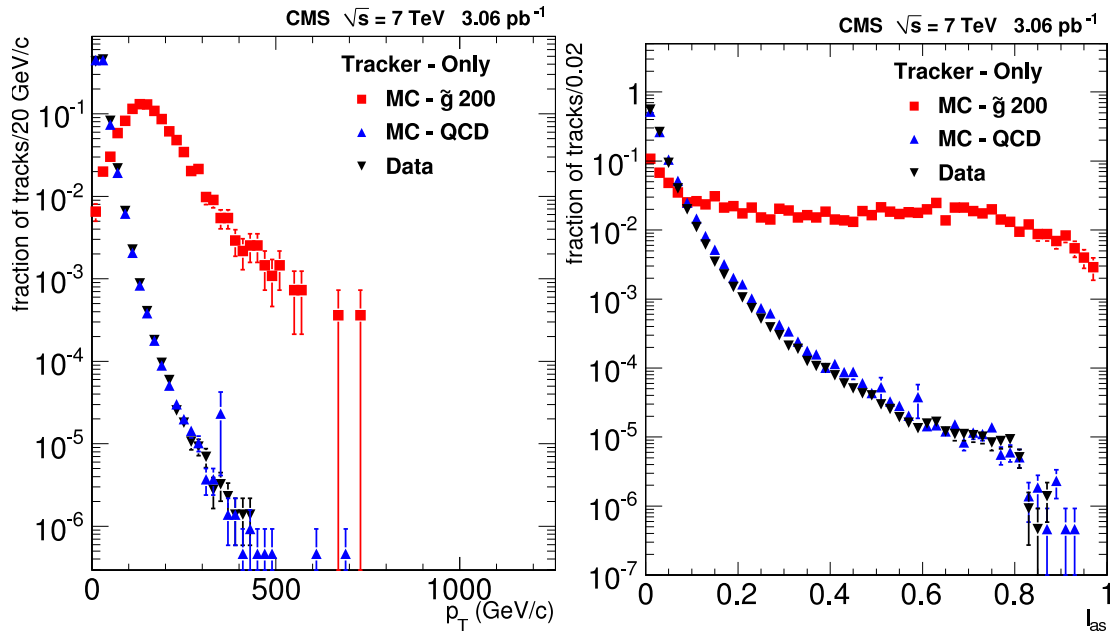


Figure 7. Data normalized distributions of p_T (left) and I_{as} (right), compared to simulations from standard QCD processes and from pair-production of \tilde{g} with a mass of 200 GeV/ c^2 .

The mass of the candidates is extracted from the measured dE/dx and p values, inverting a parametrized Bethe-Bloch fitted from data. The search is performed as a counting experiment with candidates required to have I_{as} and p_T greater than threshold values, and the candidates mass to be in the range of 75 to 2000 GeV/ c^2 .

No signal candidates are observed in the data, with 0.074 ± 0.011 expected from standard processes for the tracker-only selection, and 0.025 ± 0.004 for the tracker-plus-muon selection. Therefore cross section upper limits at the 95% CL are set on the HSCP production for two benchmark scenarios: direct production of \tilde{g} pairs and \tilde{t}_1 pairs. The signal efficiencies depend on the hadronization fractions and interactions of the resulting signal R -hadrons. A summary of cross section upper limits, set with a Bayesian method, are shown in Figure 8. The tracker-plus-muon selection set a 95% CL lower mass limit of 398 GeV/ c^2 for long-lived \tilde{g} with a $f = 0.1$ fraction of R -gluonball states, and of 202 GeV/ c^2 for long-lived \tilde{t}_1 . In a pessimistic scenario of complete charge suppression the tracker-only selection yields a \tilde{g} mass limit of 311 GeV/ c^2 .

6. Search for stopped gluinos

A significant fraction of slow charged R -hadrons, resulting from the production of long-lived gluinos, can lose sufficient energy to be stopped inside the CMS detector and may decay at later

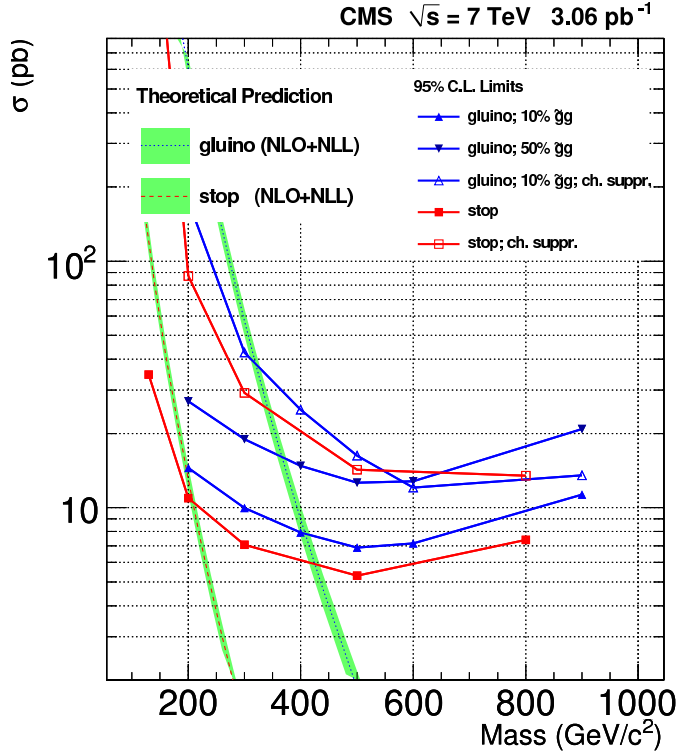


Figure 8. HSCP theoretical production cross section and observed 95% CL upper limits for different combinations of models and scenarios: pair production of supersymmetric stop and gluinos; different fractions, f , of R -gluonball hadronization states and charge suppression scenarios [17]. Only the results obtained with the most sensitive selection are reported: tracker-only for the charge suppression scenarios and tracker-plus-muon for all other cases. The bands represent the theoretical uncertainties on the cross section values.

times (with $\tilde{g} \rightarrow g\tilde{\chi}_1^0$) resulting in jet-like signals in the calorimeters, out-of-time with respect to LHC collisions. The presence of a stopped-particle signal is searched for in 62 hours of trigger live-time, following collision data corresponding to 10 pb^{-1} recorded with $1 \times 10^{32} \text{ cm}^{-2}\text{s}^{-1}$ peak luminosity. A control sample of 95 hours of trigger live-time collected during fills with $2 - 7 \times 10^{27} \text{ cm}^{-2}\text{s}^{-1}$ luminosity is used to estimate the background rates [18].

A dedicated trigger is used that requires a jet-like signal when no beam is crossing CMS, and outside a 75 ns window around beam crossings. Care is taken to reject beam-halo events, cosmic rays and calorimeter instrumental noise. Both a counting experiment and a time-profile analysis are performed for candidate events, building a probability density function (PDF) for the gluino decay signal. Figure 9 shows an example of such a PDF for a $1 \mu\text{s}$ lifetime, together with the in-orbit positions of two candidate events.

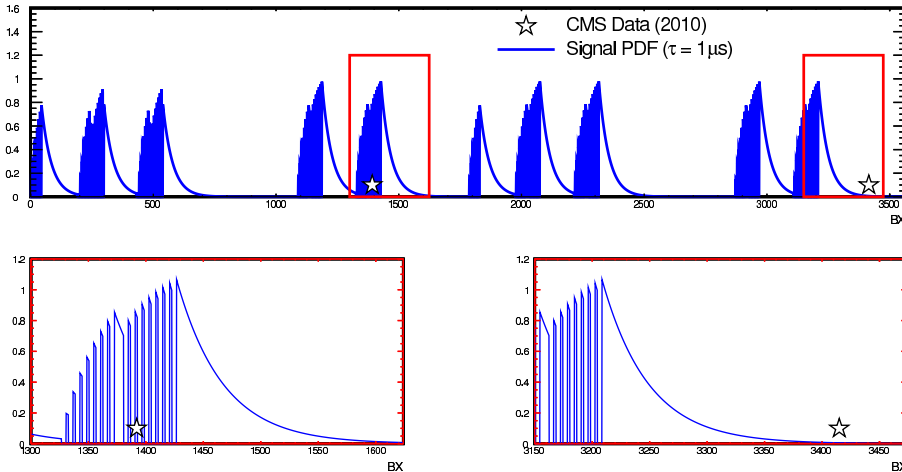


Figure 9. In-orbit positions of two observed events recorded during an LHC fill with 140 colliding bunches. The decay profile for a $1 \mu\text{s}$ lifetime hypothesis is overlaid. The bottom panels are zoomed views of the boxed regions around the two events.

Finally no excess of signal events over the expected background rates is observed in the search sample, for any lifetime hypothesis, so that 95% CL limits are set on $\sigma(pp \rightarrow \tilde{g}\tilde{g}) \times BR(\tilde{g} \rightarrow g\tilde{\chi}_1^0)$ for a given mass difference $m_{\tilde{g}} - m_{\tilde{\chi}_1^0} > 100 \text{ GeV}/c^2$, and are summarized in Figure 10. For $m_{\tilde{g}} = 300 \text{ GeV}/c^2$ lifetimes from 75 ns to $3 \times 10^5 \text{ s}$ are excluded with the counting experiment.

The excluded regions as a function of the gluino mass are plotted in Figure 11. For lifetimes between 10 μs and 1000 s $m_{\tilde{g}} < 370 \text{ GeV}/c^2$ is excluded, and if only electromagnetic (EM) interactions are considered the limit becomes $m_{\tilde{g}} < 302 \text{ GeV}/c^2$.

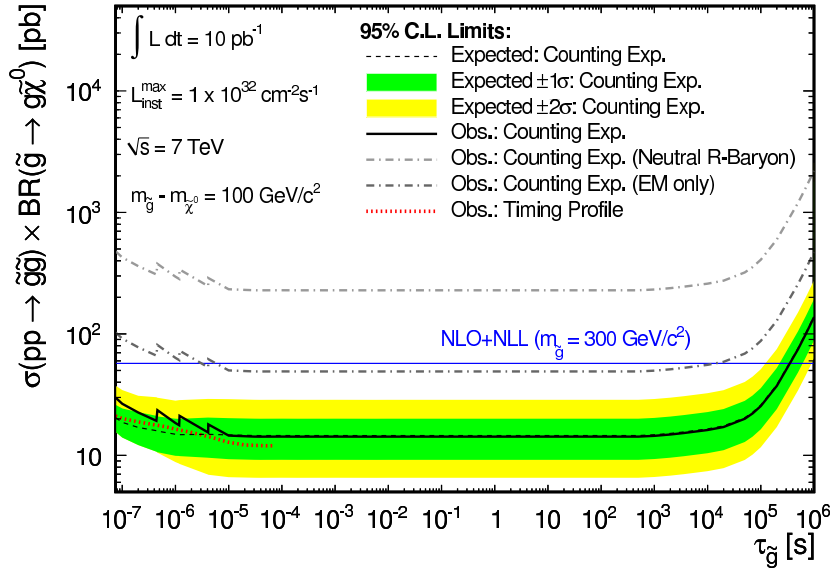


Figure 10. Expected and observed 95% CL limits on gluino pair production cross section times branching fraction as a function of the gluino lifetime from the counting experiment and the time-profile analysis. Alternative R-hadron interaction scenarios are also presented. The NLO+NLL production expectation for $m_{\tilde{g}} = 300 \text{ GeV}/c^2$ is also indicated.

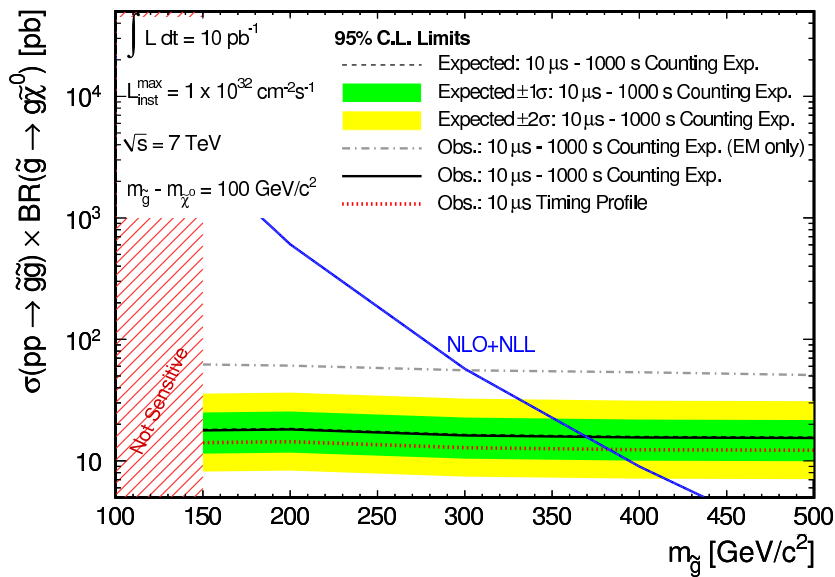


Figure 11. Upper 95% CL limits on gluino pair production cross section times branching fraction as a function of the gluino mass with strong or EM only R-hadron interactions. The $m_{\tilde{g}} - m_{\tilde{\chi}_1^0}$ difference is set at 100 GeV/c^2 and $m_{\tilde{\chi}_1^0} > 50 \text{ GeV}/c^2$ is assumed. The NLO+NLL expected production are also shown. The indicated lifetimes maximize the counting experiment and time-profile analysis sensitivity.

References

- [1] R. Adolphi *et al.* [CMS Collaboration], JINST **3** (2008) S08004.
- [2] M. Fairbairn *et al.*, “Stable massive particles at colliders”, *Phys. Rept.* **438** (2007) 1,
- [3] V. Khachatryan *et al.* [CMS Collaboration], “Search for Dijet Resonances in 7 TeV pp Collisions at CMS,” *Phys. Rev. Lett.* **105** (2010) 211801 [arXiv:1010.0203 [hep-ex]].
- [4] M. Cacciari, G. P. Salam, and G. Soyez, “The anti-k(t) jet clustering algorithm”, *JHEP* **04** (2008) 063.
- [5] CMS Collaboration, “Jet Performance in pp Collisions at $\sqrt{s}=7$ TeV”, *CMS Physics Analysis Summary CMS-PAS-JME-10-003* (2010).
- [6] T. Sjostrand *et al.*, “High-energy-physics event generation with PYTHIA 6.1”, *Computer Physics Commun.* **135** (2001) 238.
- [7] L. A. Anchordoqui, H. Goldberg, S. Nawata *et al.*, “Jet signals for low mass strings at the Large Hadron Collider”, *Phys. Rev. Lett.* **101** (2008) 241803.
- [8] U. Baur, I. Hinchliffe, and D. Zeppenfeld, “Excited Quark Production at Hadron Colliders”, *Int. J. Mod. Phys.* **A2** (1987) 1285.
- [9] P. H. Frampton and S. L. Glashow, “Chiral color: An alternative to the standard model”, *Phys. Lett.* **B190** (1987) 157.
- [10] E. H. Simmons, “Coloron phenomenology”, *Phys. Rev.* **D55** (1997) 1678.
- [11] J. L. Hewett and T. G. Rizzo, “Low-energy phenomenology of superstring-inspired E_6 models”, *Phys. Rept.* **183** (1989) 193.
- [12] E. Eichten, I. Hinchliffe, K. Lane *et al.*, “Supercollider physics”, *Rev. Mod. Phys.* **56** (1984) 579.
- [13] L. Randall and R. Sundrum, “An alternative to compactification”, *Phys. Rev. Lett.* **83** (1999) 4690.
- [14] V. Khachatryan *et al.* [CMS Collaboration], “Search for Quark Compositeness with the Dijet Centrality Ratio in pp Collisions at $\sqrt{s}=7$ TeV,” *Phys. Rev. Lett.* **105** (2010) 262001 [arXiv:1010.4439 [hep-ex]].
- [15] A. L. Read, “Modified frequentist analysis of search results (The CL(s) method)”, in *First Workshop on Confidence Limits, CERN, Geneva, Switzerland*, pp. 81–101. Jan, 2000.
- [16] V. Khachatryan *et al.* [CMS Collaboration], “Measurement of Dijet Angular Distributions and Search for Quark Compositeness in pp Collisions at 7 TeV,” arXiv:1102.2020 [hep-ex].
- [17] V. Khachatryan *et al.* [CMS Collaboration], “Search for Heavy Stable Charged Particles in pp collisions at $\sqrt{s}=7$ TeV,” arXiv:1101.1645 [hep-ex].
- [18] V. Khachatryan *et al.* [CMS Collaboration], “Search for Stopped Gluinos in pp collisions at $\sqrt{s} = 7$ TeV,” *Phys. Rev. Lett.* **106** (2011) 011801 [arXiv:1011.5861 [hep-ex]].
- [19] W. Beenakker *et al.*, “Soft-gluon resummation for squark and gluino hadroproduction”, *JHEP* **12** (2009) 041,

